Ahmadi-Naghadeh, R. *et al*. (2024). *Géotechnique* **74**, No. 6, 527–539 [https://doi.org/10.1680/jgeot.21.00198]

A laboratory characterisation of the response of intact chalk to cyclic loading

REZA AHMADI-NAGHADEH*, TINGFA LIU†, KEN VINCK‡, RICHARD J. JARDINE§, STAVROULA KONTOE‖, BYRON W. BYRNE¶ and ROSS A. MCADAM**

This paper reports the cyclic behaviour of chalk, which has yet to be studied comprehensively. Multiple undrained high-resolution cyclic triaxial experiments on low- to medium-density intact chalk, along with index and monotonic reference tests, define the conditions under which either thousands of cycles could be applied without any deleterious effect, or failure could be provoked under specified numbers of cycles. Intact chalk's response is shown to differ from that of most saturated soils tested under comparable conditions. While chalk can be reduced to putty by severe two-way displacement-controlled cycling, its behaviour proved stable and nearly linear visco-elastic over much of the one-way, stress-controlled loading space examined, with stiffness improving over thousands of cycles, without loss of undrained shear strength. However, in cases where cyclic failure occurred, the specimens showed little sign of cyclic damage before cracking and movements on discontinuities led to sharp pore pressure reductions, non-uniform displacements and the onset of brittle collapse. Chalk's behaviour resembles the fatigue response of metals, concretes and rocks, where micro-shearing or cracking initiates on imperfections that generate stress concentrations; the experiments identify the key features that must be captured in any representative cyclic loading model.

KEYWORDS: chalk; cyclic loading; fatigue; laboratory testing; triaxial

INTRODUCTION

Cyclic testing is often required to support offshore foundation design (Andersen, 2009; Jardine *et al*., 2012). Wide ranges of conditions have been investigated for sands and clays in triaxial experiments that identify cyclic failure conditions and track permanent strains, cyclic stiffness and damping ratio changes (Wichtmann *et al*., 2005; Andersen, 2015; Ushev & Jardine, 2022). If undrained, they also establish how mean effective stresses or pore pressures drift throughout cycling. Constant volume cyclic simple shear (CSS) testing is also commonly undertaken (Andersen, 2015), although CSS tests provide less complete information.

Manuscript received 13 July 2021; revised manuscript accepted 14 January 2022. First published online ahead of print 14 March 2022.
Discussion on this paper closes on 1 September 2024, for further details see p. ii.

* Formerly Department of Civil and Environmental Engineering, Imperial College London, London, UK; now Department of Construction Engineering and Lighting Science, School of Engineering, Jönköping University, Jönköping, Sweden (Orcid:0000-0002-2215-441X).
† Department of Civil Engineering, University of Bristol, Bristol, UK; formerly Department of Civil and Environmental Engineering, Imperial College London, London, UK (Orcid:0000-0002-5719-8420).
‡ Department of Civil and Environmental Engineering, Imperial College London, London, UK (Orcid:0000-0002-0990-0895).
§ Department of Civil and Environmental Engineering, Imperial College London, London, UK (Orcid:0000-0001-7147-5909).
‖ Department of Civil and Environmental Engineering, Imperial College London, London, UK (Orcid:0000-0002-8354-8762).
¶ Department of Engineering Science, University of Oxford, Oxford, UK (Orcid:0000-0002-9704-0767).
** Department of Engineering Science, University of Oxford, Oxford, UK (Orcid:0000-0003-0292-3549).

Cyclic testing has been reported on calcarenite, a very soft, sand-sized, carbonate-cemented rock. Acharya (2004) reviewed the extreme difficulty of investigating inherently variable naturally cemented samples before setting out comprehensive cyclic triaxial testing of artificially recemented reconstituted calcarenite. Comparable studies do not appear to have been reported for chalk, a similarly very soft, silt-sized carbonate rock, although limited testing is described for specific projects by Le *et al*. (2014), Coyne *et al*. (2015) and Larsen *et al*. (2017). Large-displacement CSS testing was also reported by Carrington *et al*. (2011).

This paper examines the behaviour of intact chalk under repeated loading through systematic testing of multiple, nominally identical, natural specimens. The programme supported the joint industry project 'axial-lateral pile analysis for chalk applying multi-scale field and laboratory testing' (ALPACA), which investigated how 37 tubular steel piles, such as those driven in offshore low- to medium-density chalk, behaved under axial and lateral, monotonic and cyclic loading at the research site at St Nicholas-at-Wade (SNW), Kent, UK (Jardine *et al*., 2019).

Vinck (2021) and Vinck *et al*. (2022) describe the SNW ground conditions and report the site's characterisation by comprehensive in situ profiling and monotonic laboratory testing. Sample variability posed a significant challenge, as with calcarenites, and testing focused on 20 low- to medium-density 'structured' (Leroueil & Vaughan, 1990) high-quality specimens from a single location and depth.

The intact chalk's response controls the piles' resistance to lateral cyclic loading and has implications for other applications, including spread or 'gravity-base' foundations. Noting that the strain-gauged ALPACA project's test piles' lateral responses were found to be governed by the upper 3 m of chalk, the study focused on block samples taken several metres from the piles, at $\approx 1{\cdot}4$ m depth, 4·6 m above the water table. The block samples showed similar shear strengths to, but lower initial stiffness than, the deeper chalk layers. Stress-controlled, mainly low-strain, cyclic triaxial tests established behaviour

from both 'in situ' and 'elevated by 300 kPa' initial mean effective stress (p'_0) levels, covering the mean stress range anticipated around the lateral test piles. Noting that pile driving creates an annulus of destructured 'putty' around pile shafts, Liu *et al.* (2022) examined separately the cyclic behaviour of dynamically destructured chalk, which determines how shaft capacities degrade under high-level axial cycling.

SAMPLING, SPECIMEN PREPARATION AND CHALK PROPERTIES

Vinck *et al.* (2022) describe how weathered material has been removed at SNW, exposing CIRIA grade B2, very weak to weak, low- to medium-density, white structured chalk, which has closed to slightly open stained joints and horizontal beds of 250 mm average thickness. Micro-fissures, which are mainly vertically oriented and spaced 10 to 25 mm apart, were identified over the full sampled chalk profile. Block samples were carefully trimmed, preserved and prepared in the laboratory for cyclic testing, meeting or exceeding ASTM (2019) rock testing requirements. Specimens showed initial triaxial suctions of 70 to 80 kPa and generally higher shear wave velocities than those measured in situ, suggesting minimal overall disturbance. All laboratory tests were performed on samples preserved at in situ water contents of $\approx 30\%$ with average bulk density of 1·92 Mg/m^3. The degree of saturation was close to unity at 1·4 m depth and in situ mean effective stress p' was calculated as 42 kPa assuming K_0 of 0·6 and taking suction ≈ 30 kPa, based on a tensiometer installed above the water table (Vinck *et al.*, 2022).

The SNW chalk presents, when tested under in situ and 300 kPa higher effective stress levels, extremely brittle and ultimately dilative monotonic triaxial compression behaviour. Peak undrained triaxial shear strengths, S_u, exceeding 1 MPa, develop after as little as 0·1% axial strain, before bifurcation and cracking leads to strikingly brittle post-peak behaviour. The chalk develops significant creep strains when held under constant effective stresses that are significantly greater than those acting in situ. Loading rates also affect stiffness and oedometer vertical yield stresses markedly, but have less influence on shear strength. The intact chalk also transitions towards showing ductile behaviour after consolidation to $p' \geq 2$ MPa.

APPARATUS, PROCEDURES AND PROGRAMME

Apparatus

Hydraulic stress path apparatus was employed to test 38 mm dia., 76 mm high, specimens. Diametrically opposed pairs of vertically mounted linear variable differential transducers (LVDTs) (with optimal precision around 0·1 μm) were installed over the central 50 mm lengths to measure local axial strains, while external sensors measured global straining. Pore pressures were measured at the specimen bases in tests conducted sufficiently slowly for full pore pressure equalisation during undrained monotonic and cyclic loading. A suction cap and half-ball connection system centralised the loading of the top platen. Double layers of latex membrane smeared with high-vacuum grease were deployed at the tops and bases of the specimens to minimise stress non-uniformity (Vinck *et al.*, 2019). The equipment could apply deviator stress (q) of up to 4 MPa and cell pressures up to 750 kPa. Triaxial extension failure would require cell pressures of up to 4 MPa, so the programme was limited to compressive loading paths, without any two-way loading.

Procedures and programme

Sample preparation is challenging with chalk. System compliance effects are highly significant, while end-parallelism and flatness are especially important (Jardine *et al.*, 1985). Specimen imperfections can lead to misleading stiffness data and affect shear strengths with brittle cemented soils, as examined by Maqsood *et al.* (2019) with cemented sands of similar shear strength. Preliminary tests confirmed that even slight irregularities in specimen ends led to premature failure and unrepresentative stiffness. All the undrained monotonic and cyclic loading tests in this study were conducted on nominally identical specimens, isotropically consolidated to either in situ ($p'_0 = 42$ kPa) or 300 kPa higher than in situ ($p'_0 = 342$ kPa) mean effective stresses. The latter tests approached the system's cell and ram pressure limits. Tests in which the axial strains given by the opposing local LVDTs showed significantly different trends were repeated.

Table 1. Undrained monotonic peak strengths and the adopted mean S_u values

Test	e_0*	p'_0: kPa	q_f: kPa	S_u: kPa
IM-1	0·839	42	2322	1200 (±50)
IM-2	0·835	42	2511	
EM-1	0·802	342	2328	1300 (±150)
EM-2	0·808	342	2925	

*Void ratio prior to isotropic consolidation

Despite being sub-sampled from large blocks, scope existed for significant natural deviation between the distributions of micro-fissures and other natural imperfections. Isotropically consolidated and undrained (CIU) tests conducted from in situ ($p'_0 = 42$ kPa) conditions indicated representative mean undrained S_u values of ≈ 1200 kPa, and ≈ 1300 kPa under the elevated $p'_0 = 342$ kPa conditions (see Table 1). Variations of ± 12% relative to the means were assessed from multiple initial tests on 'identical' specimens. Substantial, greater variations are often found between nominally identical samples of natural cemented carbonate rocks by, for example, Acharya (2004). Table 2 summarises the ranges of average, q_{mean}, and cyclic, q_{cyc}, deviatoric stresses applied, where $q = (\sigma'_v - \sigma'_h)$ and $p' = (\sigma'_v + 2\sigma'_h)/3$, with both absolute and normalised (by appropriate $2S_u$) values. The test codes comprise

(*a*) letters 'I' for in situ or 'E' for 'elevated' consolidation stresses
(*b*) letter 'M' for monotonic or 'Cy' for cyclic loading
(*c*) group letter A, B, C or D for cyclic tests, signifying the maximum q applied in the 'ICy' series, and letter E or F in the 'ECy' series, in ascending order
(*d*) within each A to D group, a numeral signifying applied q_{cyc} level, in ascending order
(*e*) letter 'R' for any repeated test.

Figure 1 presents the cyclic triaxial tests' typical loading–time history. Samples were saturated by applying back-pressure (usually 300 kPa) until B exceeded 0·95, while maintaining $p'_0 = 42$ kPa; elevated pressure tests were consolidated to $p'_0 = 342$ kPa. All were kept at constant effective stress until creep rates fell below 0·005% per day, which took at least 48 h. The intact chalk's monotonic behaviour is considered below, before describing the cyclic tests and their interpretation in greater detail.

Undrained monotonic behaviour

Two pairs of monotonic CIU compression tests are listed, conducted from in situ and elevated pressures while maintaining constant σ_r and applying external straining at 5% per

Table 2. Summary of cyclic triaxial test conditions and parameters

Test	e_0*	q_{mean}: kPa	$q_{mean}/(2S_u)$	q_{cyc}: kPa	$q_{cyc}/(2S_u)$	$q_{max}/(2S_u)$
ICy-A1	0·847	760	0·32	365	0·15	0·47
ICy-B2	0·883	1225	0·51	250	0·10	0·61
ICy-B3	0·862	910	0·38	560	0·23	0·61
ICy-B4	0·868	750	0·31	730	0·30	0·62
ICy-C1	0·880	1575	0·66	250	0·10	0·76
ICy-C1-R	0·892	1575	0·66	250	0·10	0·76
ICy-C2	0·880	1225	0·51	600	0·25	0·76
ICy-C3	0·853	1050	0·44	760	0·32	0·75
ICy-C4	0·869	910	0·38	910	0·38	0·76
ICy-D1	0·885	1850	0·77	240	0·10	0·87
ICy-D2	0·880	1575	0·66	600	0·25	0·91
ICy-D2-R	0·871	1575	0·66	600	0·25	0·91
ICy-D3	0·880	1225	0·51	950	0·40	0·91
ICy-D4	0·849	1087	0·45	1087	0·45	0·91
ECy-E1	0·837	975	0·38	975	0·38	0·76
ECy-F1	0·795	1220	0·47	1220	0·47	0·94

*Void ratio prior to isotropic consolidation

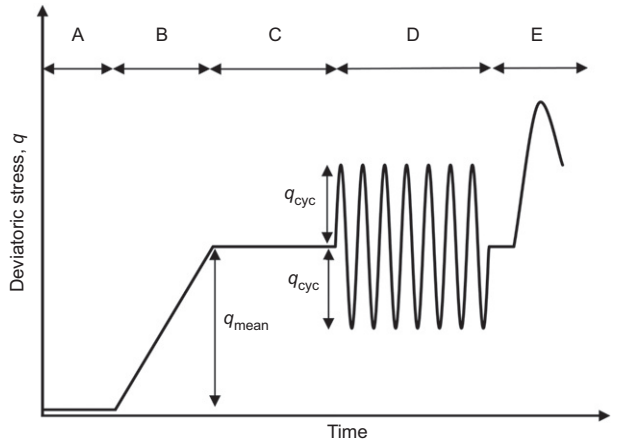

Fig. 1. Schematic diagram of testing stages: A – isotropic saturation and consolidation; B – pre–shearing; C – creep; D – cyclic loading; E – post-cyclic monotonic shearing on unfailed samples; stages B to E all undrained

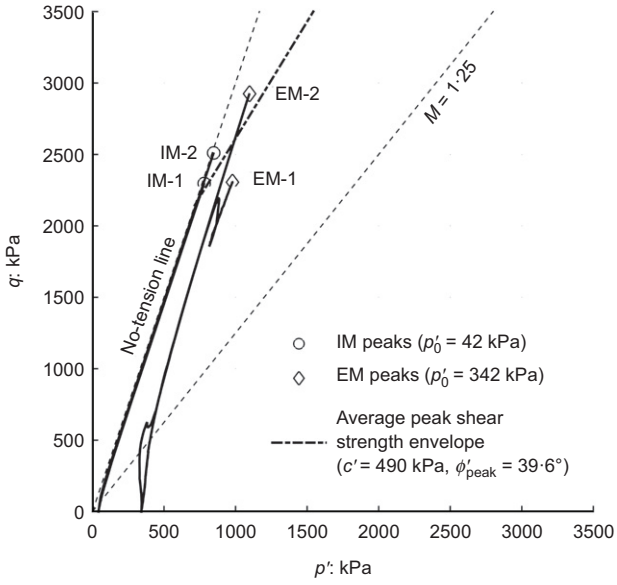

Fig. 2. Pre-yielding undrained effective stress paths and peaks for the monotonic CIU triaxial tests under in situ (p'_0 = 42 kPa) and elevated (p'_0 = 342 kPa) stresses (average peak strength envelope from Vinck *et al.* (2022))

day that allowed full definition of initial small-strain behaviour. System compliance and specimen imperfections led to five or more times lower local strain rates until failure commenced. Figs 2 and 3 present the four tests' q–p' effective stress paths and examples of the paired tests' similar overall stress–strain (q–ε_a) curves, and pore pressure–strain curves. The effective stress paths of the lower pressure tests travelled close to the no-tension line limit implicit in all triaxial testing, which has a 3 : 1 gradient, before reaching failure. Only modest pore pressure changes (30 kPa, see Table 3) developed up to peak deviator conditions and strong reductions followed post-peak as the samples failed and fractures tried to open. The elevated pressure (p'_0 = 342 kPa) tests showed, on average, higher peak shear strengths. They also followed more steeply inclined effective stress paths, developing greater (on average 175 kPa) positive pressures up to peak, and less dilatant post-peak, pore pressure changes. These features are interpreted by Vinck *et al.* (2022) as reflecting the closure of minor fissures and micro-cracks during consolidation. Such stiffness increases with strain are unusual with soils, but are observed in gravels and soft rocks containing micro-fissures (see examples by Kohata *et al.* (1997) or Tatsuoka *et al.* (1999)). Micro-computed tomography (CT) scanning or other techniques would be required to test definitively the conjecture that micro-flaws contribute to the concave initial (locally sensed) stress–strain curves developed in several tests. Higher stiffnesses were generally observed in the elevated pressures tests which, as described later, showed stiffnesses reducing more markedly with strain.

Vinck *et al.* (2022) report best-fit failure parameters covering the in situ p'_0 to $p'_0 + 300$ kPa range from 41 drained and undrained monotonic triaxial tests conducted at depths down to 18 m, as shown in q–p' co-ordinates in Fig. 2. The peak envelope corresponds to Mohr–Coulomb c' = 490 kPa and ϕ'_{peak} = 39·6°. The failures were markedly brittle, reflecting sudden losses in bond strength (or true cohesion) and the formation, or mobilisation, of discontinuities. Higher pressure tests show a curved envelope with behaviour becoming progressively more ductile with increasing confining pressure. The critical state M = 1·25 (equivalent to $\phi'_{cs} \approx 31°$), indicated on Fig. 2, matches that of chalk destructured by dynamic compaction (Liu *et al.*, 2022). Overall, the SNW chalk's monotonic behaviour is broadly consistent with that of cemented calcarenites, transitioning from being remarkably brittle towards ductile in response to raising confining pressures, as captured by the Lagioia & Nova (1995) critical-state based model.

Undrained cyclic testing

The undrained cyclic loading tests were characterised by the average q_{mean}, which was applied slowly before cyclic loading, and the amplitude q_{cyc} of the sinusoidally varying cycles defined in Fig. 1. In each test, the desired q_{mean} value (as listed in Table 2) was applied by undrained loading at a 5% external axial strain per day. Specimens were held undrained at their q_{mean} values until local axial strain rates fell below 0·005%/day, which allowed their subsequent cyclic responses to be distinguished from creep induced by applying q_{mean}. Table 3 summarises the samples' conditions at the end of their 'pre-shearing plus creep' stages. Also included for comparison are the outcomes of the four monotonic shearing tests discussed above. The in situ p'_0 (42 kPa) tests displayed relatively modest (up to 36 kPa) changes in pore pressure and far larger (broadly 210 to 610 kPa) increases in p' during pre-loading to their various q_{mean} values. The axial strains developed during creep stages generally grew with q_{mean}. Dividing the overall strain increments into q_{mean} indicates long-term 'overall Young's moduli', E^u, ranging from 0·4 to 1·1 GPa that reflect stiffness non-linearity and the creep strains. This wide range reflects variable degrees of micro-fissuring between specimens and, in some cases, the impact of non-uniform axial straining.

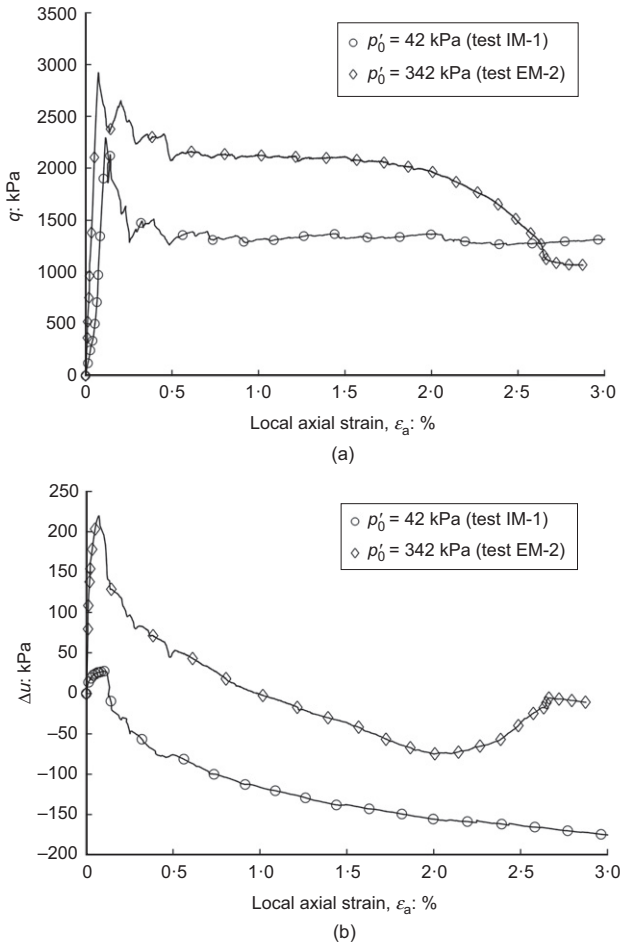

Fig. 3. Monotonic CIU triaxial tests under in situ and elevated stresses: (a) deviatoric stress and (b) excess pore water pressure plotted against local axial strains

Differences between the (diametrically opposed) pairs of strain measurements indicate the degree of strain non-uniformity. Tests by Maqsood *et al.* (2019) tests on cemented sands showed lower than representative peak shear strengths in cases where the ratio of the lower strain to the larger fell below ≈0·5. Tests ICy-C1 and ICy-D2-R showed ratios below this limit and were not included in later cyclic interpretation.

The cyclic laboratory study was intended to match the ALPACA lateral pile loading experiments. The field tests employed one-way lateral cycling with biased mean loads as this promotes more marked permanent pile deflections and rotations than symmetrical two-way cyclic loading. The field pile tests ran at ≈0·16 Hz and were mostly completed within 1 day. However, the triaxial systems employed could neither control the desired cyclic stresses accurately nor ensure representative pore pressure measurements at the same rates. Longer, 300 s, periods were adopted to achieve stress control to within ±1 kPa and reliable pore water pressure measurements. While Vinck *et al.* (2022) note that the chalk's triaxial shear strengths are relatively insensitive to strain rate, the laboratory tests could lead to lower cyclic stiffness and strengths than the faster field experiments. Tests were limited

Table 3. Final q and p' values, pore pressure changes Δu, paired local axial strains and ratio between smaller to larger axial strain at the peak strengths (q_f) of the monotonic tests or at the end of 'pre-shear and creep' stages (q_{mean}) of the cyclic tests

Test	q_f or q_{mean}: kPa	p'_f or p'_{mean}: kPa	Δu: kPa	Smaller ε_a: %	Larger ε_a: %	Mean ε_a: %	Smaller/larger ε_a
IM-1	2322	789	27	0·077	0·162	0·119	0·48
IM-2	2511	847	33	0·29	0·37	0·33	0·78
EM-1	2328	986	132	0·042	0·080	0·061	0·53
EM-2	2925	1098	219	0·072	0·078	0·075	0·92
ICy-A1	760	262	33	0·081	0·095	0·088	0·85
ICy-B2	1225	423	27	0·07	0·18	0·12	0·39
ICy-B3	910	309	36	0·095	0·17	0·13	0·56
ICy-B4	750	258	34	0·17	0·19	0·18	0·89
ICy-C1	1575	535	32	0·15	0·68	0·41	0·22
ICy-C1-R	1575	540	27	0·11	0·19	0·16	0·58
ICy-C2	1225	421	29	0·123	0·21	0·16	0·58
ICy-C3	1050	360	32	0·155	0·19	0·17	0·81
ICy-C4	910	311	34	0·099	0·117	0·088	0·85
ICy-D1	1850	622	35	0·23	0·37	0·30	0·62
ICy-D2	1575	533	34	0·12	0·158	0·14	0·76
ICy-D2-R	1575	536	31	0·07	0·19	0·13	0·37
ICy-D3	1225	417	33	0·163	0·187	0·17	0·87
ICy-D4	1087	376	28	0·15	0·35	0·25	0·43
ECy-E1	975	546	121	0·038	0·051	0·045	0·75
ECy-F1	1220	571	178	0·046	0·078	0·062	0·59

Table 4. Strains, pore pressure changes, stiffness and damping ratio variations during cyclic loading, considering changes from the first cycle up to the N_f cycle, or final cycle in the unfailed tests

Test	$q_{mean}/(2S_u)$	$q_{cyc}/(2S_u)$	$q_{max}/(2S_u)$	Imposed cycles, N_{max}	N_f*	Overall ε_a: %	ε_a/N_f: %	Overall Δu: kPa	Secant cyclic $E_{sec}^{u,cyc.}$: GPa	Damping ratio, D: %†
ICy-A1	0·32	0·15	0·47	4278	Unfailed	≈0	≈0	−3	3·9→4·2	3·1→3·8
ICy-B2	0·51	0·10	0·61	4816	Unfailed	≈0·05	$1{\cdot}1\times10^{-7}$	−6	4·0→3·6	4·7→4·4
ICy-B3	0·38	0·23	0·61	4808	Unfailed	≈0·04	$0{\cdot}9\times10^{-7}$	+1	3·8→4·9	4·7→16·7
ICy-B4	0·31	0·30	0·62	4303	Unfailed	≈0·04	$0{\cdot}9\times10^{-7}$	+1	3·5→3·8	6·4→15·5
ICy-C1	0·66	0·10	0·76	4626	Unfailed	≈0·07	$1{\cdot}6\times10^{-7}$	<1	2·5→2·3	5·4→2·7
ICy-C1-R	0·66	0·10	0·76	6415	Unfailed	≈−0·01	$0{\cdot}2\times10^{-7}$	−8	5·3→5·3	2·1→2·3
ICy-C2	0·51	0·25	0·76	309	293(A, B)	0·02	$6{\cdot}8\times10^{-5}$	−19	3·3→4·2	3·4→7·4
ICy-C3	0·44	0·32	0·75	367	283(B)	0·07	$2{\cdot}5\times10^{-4}$	−42	3·1→4·5	4·3→3·8
ICy-C4	0·38	0·38	0·76	1162	1108(A)	0·15	$1{\cdot}4\times10^{-4}$	−4	3·5→2·3	3·5→4·4
ICy-D1	0·77	0·10	0·87	220	219(A, B)	0·004	$1{\cdot}8\times10^{-5}$	−0·3	2·2→2·2	6·9 ‡→4·0
ICy-D2	0·66	0·25	0·91	4	3(A, B)	−0·0005	$-1{\cdot}7\times10^{-4}$	−0·2	4·1→4·1	3·4→3·1
ICy-D2-R	0·66	0·25	0·91	64	41(A, B)	0·005	$1{\cdot}2\times10^{-4}$	0·7	4·6→4·5	2·4→2·1
ICy-D3	0·51	0·40	0·91	238	181(A, B)	0·12	$6{\cdot}6\times10^{-4}$	−6·2	2·9→2·4	3·7→9·3
ICy-D4	0·45	0·45	0·91	130	71(A)	0·02	$2{\cdot}8\times10^{-4}$	−17	2·0→3·5	7·6→16·3
ECy-E1	0·38	0·38	0·76	3180	3141(A)	0·71	$2{\cdot}3\times10^{-4}$	68	3·7→2·0	3·9→30·5
ECy-F1	0·47	0·47	0·94	33	5(A)	0·05	$1{\cdot}0\times10^{-2}$	55	5·1→3·4	5·5→22·6

*Superscripts (A) and (B) denote the applied cyclic failure criteria.
†Damping ratio calculated as: $D = A_{loop}/(4\pi A_{elastic})$; A_{loop} – area enclosed by a stress–strain (q–ε_a) loop for a complete sinusoidal stress cycle; $A_{elastic}$ – unloading half-cycle elastic triangle area with height as q_{cyc} ($= (q_{peak} - q_{trough})/2$) and width as cyclic strain ($= (\varepsilon_{peak} - \varepsilon_{trough})/2$).
‡Relatively high damping ratio partly due to less uniform cyclic stress control applied in the first cycle.

to 6500 cycles (or 23 days of cycling) to enable feasible testing timescales.

Cyclic failure is routinely defined as occurring when cyclic triaxial strains exceed limits that vary from 5% double-amplitude axial strain in undrained symmetrical two-way tests (Ishihara, 1996) to 10% shear strain conditions (Andersen, 2015). However, such limits are inappropriate with chalk, which can fail abruptly at 0·1% strain after only minor changes in pore water pressure. Cyclic failure was instead defined by whichever of the two criteria below was satisfied first

(*a*) criterion A: sharply rising strain rates that add > 0·1% over a single cycle
(*b*) criterion B: absolute monotonic changes Δu in pore pressure exceeding the pre-shearing consolidation pressure – 42 kPa and 342 kPa, respectively, for the 'in situ' and 'elevated' pressure tests.

Loading continued until either failure occurred or the cycling durations became excessive. Samples that survived without failure were maintained at constant q_{mean} until axial creep strain rates fell below 0·005%/day, before being compressed to undrained failure at 5%/day.

UNDRAINED CYCLIC OUTCOMES

The outcomes are summarised in Table 4, which lists overall axial strains, pore pressure changes and ranges of stiffness and damping ratio experienced up to either the onset of cyclic failure or, for unfailed samples, the end of cycling.

Tests from in situ p′

Figure 4 presents an overview of the in situ p' (ICy) series, showing the number of cycles required to reach failure (N_f) for each q_{mean} and q_{cyc} combination, normalised by $2S_u$. N_{max} signifies the number of complete cycles imposed and cases annotated as $> N_{max}$ did not fail. The nominal $N_f = 1$ contour line, which is plotted from $q_{cyc} = 0$, $q_{mean} = 2S_u$ to $q_{cyc} = 2S_u$, $q_{mean} = 0$, neglects any potential strain rate effects.

The degree of repeatability can be gauged by considering first test ICy-C1, and its repeat test ICy-C1-R. As shown in Table 4, the (higher quality) second specimen with better strain uniformity (see Table 3) developed significantly smaller strains (by ≈0·08%), higher stiffness and lower damping ratios, confirming that imperfect sample ends bias the results. However, both specimens survived several thousand cycles without failing. The next repeated test, ICy-D2-R, was conducted after ICy-D2 had failed after just four cycles. Although the second check test failed after 41 cycles, the first experiment (ICy-D2) indicated better local strain uniformity (see Table 3) and was considered more representative. While these cases confirm broadly comparable outcomes from repeated tests, the precise numbers of cycles to failure and detailed evolution of strains under cycling reflect the ± 12% scatter noted earlier in the monotonic S_u values. Similar problems are encountered with cyclic tests on concretes and on cemented soils. Probabilistic approaches have been developed that may be beneficial when suitably large datasets are available (see Vipulanandan & Ata (2000)).

The scatter observed in nominally identical cyclic and monotonic tests precluded applying any elaborate contouring scheme for the number of cycles (N_f) required to cause failure. Recalling that loading covered only one quadrant of the possible interactive stress conditions, a tentative fan of linear N_f contours is included in Fig. 4 to indicate the main trends applying between 1 and 3000 cycles, whose derivation is

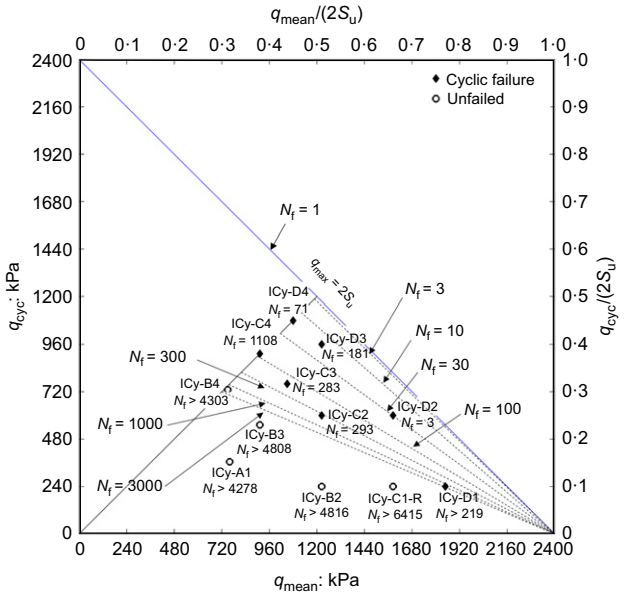

Fig. 4. Cyclic interaction diagram for ICy series, showing stress conditions in q_{cyc}–q_{mean} space and the interpreted contours of number of cycles to failure

described further later. No cyclic failure was observed in all the experiments positioned to the left of the $N_f = 3000$ contour, but several individual failure test points deviate from the interpreted contours by up to 0·05, or 10% of the maximum q applied, in the $q_{cyc}/(2S_u)$–$q_{mean}/(2S_u)$ diagram. In particular, ICy-D1 failed earlier than expected, after 219 cycles; it also developed relatively high pre-shear and creep strains (see Table 3) and low cyclic stiffness (see Table 4). This specimen may have been intrinsically weaker than average. Although substantially more tests would be required to define more definitive contour patterns or apply any probabilistic approach, it is important to recall that the contours applying to most geomaterials curve downwards in the left-hand, two-way, cyclic region (Andersen, 2015) and also that extreme displacement-controlled two-way CSS testing can reduce chalk to soft putty (Carrington *et al.*, 2011).

Before considering the detailed outcomes, it is useful to consider the stiffness–strain trends identified from the 'pre-shearing', 'creep' and 'first cycle' stages of the typical 'in situ' and 'elevated' pressure tests ICy-D3 and ECy-F1 presented in Fig. 5. ICy-D3 displayed a concave (stiffness increasing with q) trend during its initial loading, with an initial undrained Young's modulus $E^u \approx 0{\cdot}8$ GPa that rose markedly once $q > 500$ kPa. In contrast, the elevated pressure test gave $E_u^{max} = 9{\cdot}6$ GPa at its outset followed by a convex (stiffness falling with strain) non-linear response as q_{mean} increased. Significant creep developed over the 48 h constant q_{mean} pause periods. The stiffnesses ($E_{sec}^{u,cyc}$) mobilised on cycling from q_{mean} were significantly higher from the outset (given as $N = 1$ in Table 4) than the monotonic values and showed modest changes up to the onset of failure. The authors interpret these stiffness variations as being due to micro-fissure closure occurring during the pre-shearing and creep stages.

The chalk's response to high-level cyclic loading is illustrated in Figs 6 and 7 by tracking the evolution of applied deviatoric stress, axial strain and pore pressure with N for a typical unstable test (ICy-D3) as well as the effective stress path followed up to the onset of failure. Fig. 8 plots the corresponding changes in the secant undrained cyclic Young's modulus and damping ratio, which were defined from the span in strains and stresses between the peaks and troughs of each cycle. The key points are given below.

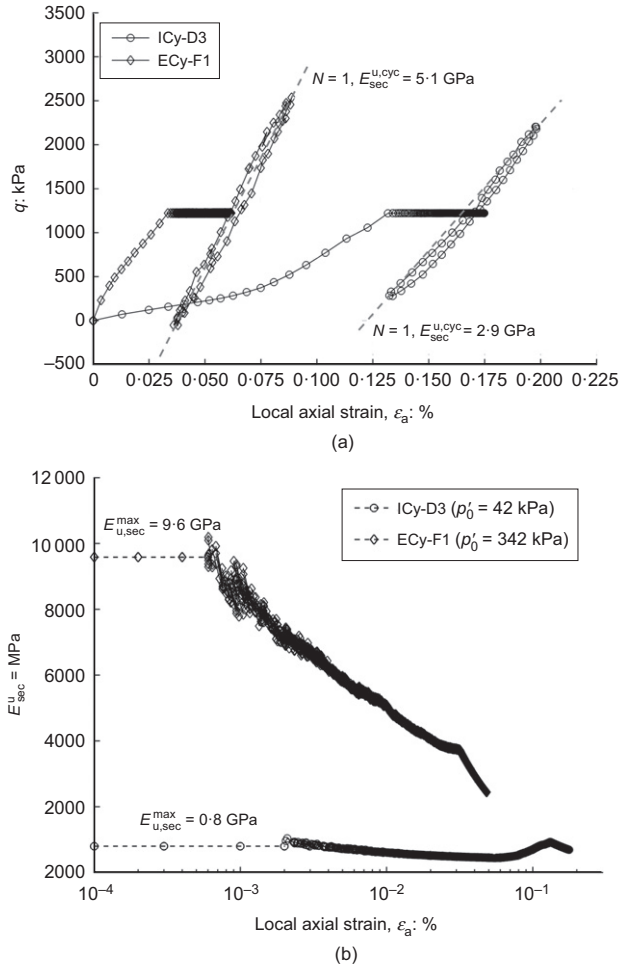

Fig. 5. Tests ICy-D3 and ECy-F1: (a) deviatoric stress–axial strain response during monotonic pre-shearing, creep and the first cycle; (b) undrained Young's moduli decay against local axial strain over pre-shearing to q_{mean}

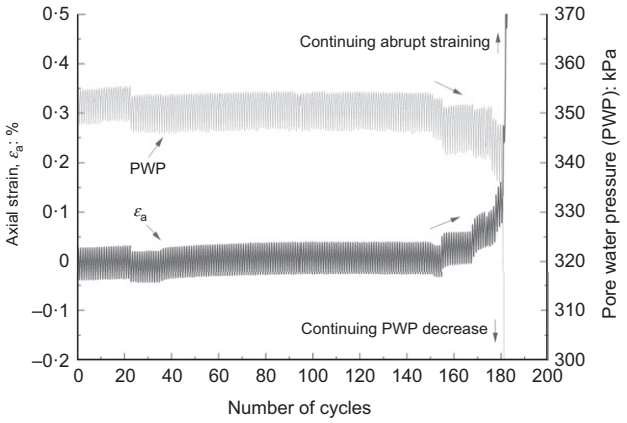

Fig. 6. Unstable ICy-D3 test: variation of axial strain and pore water pressure against number of cycles up to failure ($N_f = 181$)

(*a*) Brittle failure occurred after 181 regular cycles, after which the target $q_{max} = q_{cyc} + q_{mean}$ could not be sustained.

(*b*) The recorded strains and pore pressures showed little or no sign of impending instability, until $N \approx 150$. Relatively modest changes of around 0·1% axial strain and −6 kPa, respectively, developed over the following 30 cycles, followed by abrupt and brittle failure.

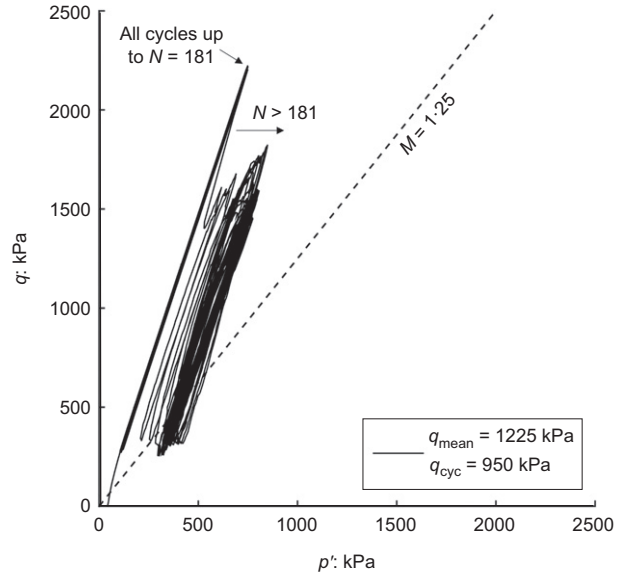

Fig. 7. Effective stress path for unstable test ICy-D3

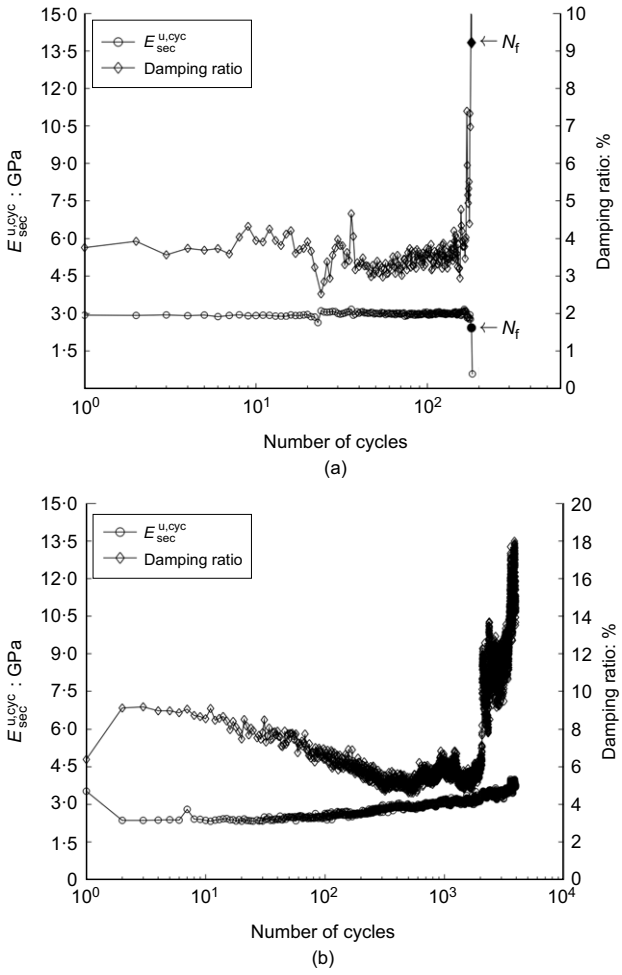

Fig. 8. Examples of cyclic secant stiffness and damping ratio plotted against number of cycles: (a) unstable ICy-D3 and (b) stable ICy-B4

(*c*) Little change was seen in either the damping ratio (which remained at around 4%) or the cyclic stiffness, which remained relatively high at around 2·9 GPa, well above the typical initial monotonic stiffness trend shown in Fig. 5, until degradation set in over the last 30 cycles.

(*d*) The effective stress path showed no leftward drift, as is usual in tests on saturated soils. Instead, the paths remained within a tight band close to the non-tension limit until cyclic loading degraded the cemented chalk's internal structure sufficiently for abrupt failure to occur under the imposed q_{max}.

The equivalent stable experiments showed minimal changes in axial strain and pore pressures. For example, the typical ICy-B4 test strained by just 0·05% over 16 days of cycling gave an overall strain rate lower than the $< 0{\cdot}005\%$/day residual creep rate tolerated before the start of cycling, while its pore pressure drift was < 1 kPa. As shown in Fig. 8, this specimen's behaviour could be considered as nearly linear visco-elastic, with cyclic stiffnesses around 3·5 GPa initially, which exceeded the monotonic CIU test's 0·8 GPa stiffness (see Fig. 5) and gradually rose to $\approx 3{\cdot}8$ GPa as cycling progressed. The damping ratio fluctuated from around 6·4% initially to exceed 10% as N increased, reflecting the relatively high q_{cyc}/q_{mean} ratio (close to unity, see Table 4).

All but two of the unstable cyclic tests failed according to the permanent strain criterion. However, tests ICy-C3 and ICy-D4 showed significant pore pressure reductions and met criterion B at an earlier stage. Fig. 9 illustrates the two-stage failure that commenced after 235 cycles in ICy-C3, when the pore pressures fell abruptly by 42 kPa while the axial strain appeared to decrease, possibly due to slipping on partly formed discontinuities. The pore pressures recovered slightly before reducing again after cycle 283 and fell, by ≈ 250 kPa, before brittle failure started at 312 cycles and the permanent strain criterion (A) was satisfied. Similar patterns are presented in Fig. 10 for ICy-D4, which is discussed further below in relation to the 'elevated' pressure test, ECy-F1.

Elevated pressure tests

As demonstrated in Figs 3 and 5 and summarised in Table 3, specimens consolidated 300 kPa above in situ stresses exhibited higher initial stiffness and larger positive excess pore water pressures during shearing. Figs 10 and 11 compare the local axial strain and pore pressure trends for ECy-E1 and ECy-F1 with ICy-C4 and ICy-D4, which applied comparable normalised $q_{mean}/(2S_u) = q_{cyc}/(2S_u)$ ratios of $0{\cdot}38$ and $0{\cdot}46 \pm 0{\cdot}01$, respectively (see Table 2). Also denoted are the numbers of cycles to failure (N_f) and the corresponding cyclic pore pressure amplitudes (u_f^{ampl}), overall axial strain ($\Delta\varepsilon_a$) and pore pressure (Δu) increments up to failure. The number of cycles to failure (N_f) for the elevated pressure tests were found broadly, but not precisely, compatible with the contour diagram interpreted tentatively from the 'in situ' pressure tests in Fig. 4. While the lower amplitude ECy test appears to have sustained more cycles than might be expected before failing, the ECy tests' permanent strain ratios (ε_a/N_f) are broadly consistent with the ICy outcomes (see Table 4).

The cyclic experiments all showed modest permanent strain development up to the onset of brittle failure. However, the ECy specimens' pore pressures oscillated with larger amplitudes and overall pore pressure rises of 55 and 68 kPa developed in ECy-F1 and ECy-E1, respectively, that led to their effective stress paths drifting leftwards prior to failure. Noting their less dilatant failures, the ECy tests manifested marginally more 'soil-like' responses than when cycled from 'in situ' stresses. However, their failures occurred before the drifting effective stress paths engaged the chalk's monotonic shear failure criterion.

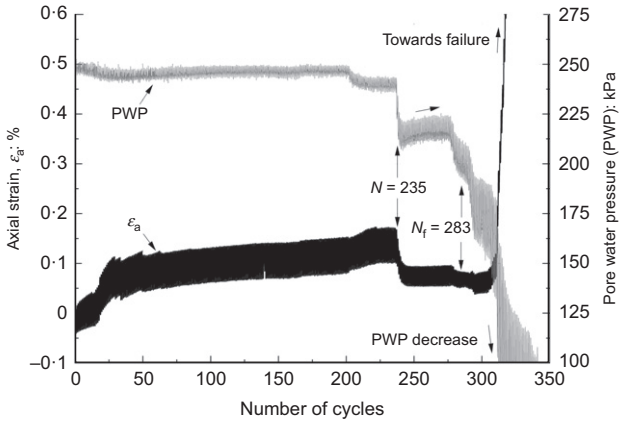

Fig. 9. Example of test ICy-C3 with multiple stage failure: axial strain and pore water pressure plotted against number of cycles

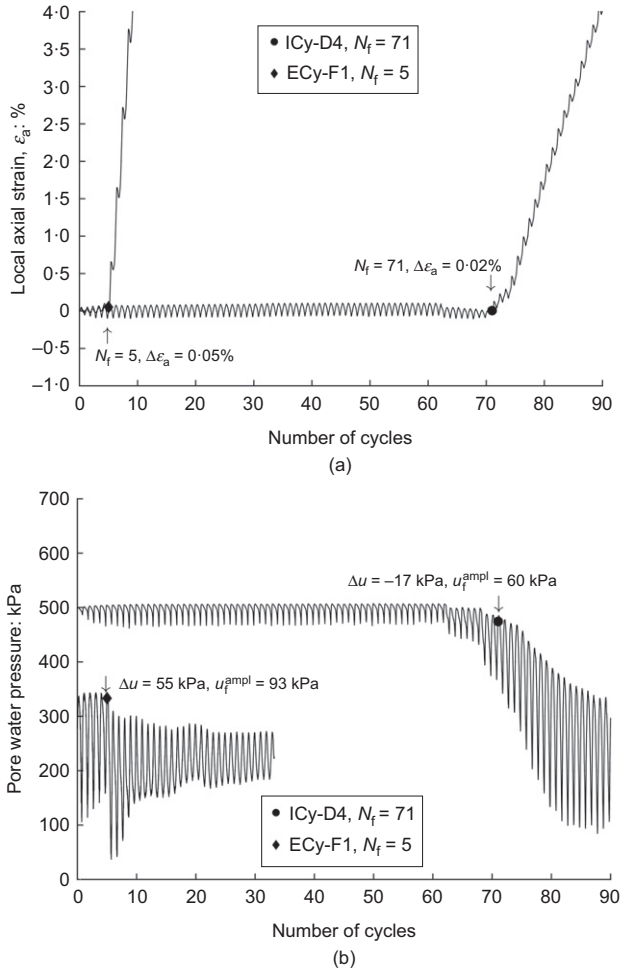

Fig. 10. (a) Cyclic axial strain and (b) pore water pressure trends for tests ICy-D4 and ECy-F1 performed at in situ and elevated stresses, denoting axial strains (ε_a) and pore water pressure (PWP) at the end of the N_f cycle, and the PWP amplitudes (u_f^{ampl}) of the N_f cycle

Cyclic strain accumulation and stiffness

Table 4 indicates three patterns of cyclic strain accumulation. The permanent strains recorded at each mid-cycle of the tests with lowest loading level, ICy-A1 to ICy-C1-R inclusive, are illustrated in Fig. 12(a), which excludes test ICy-C1 due to its earlier discussed pre-shearing strain non-uniformity. Some tests showed flat lines, while others grew with gentle gradients and some showed an initial offset

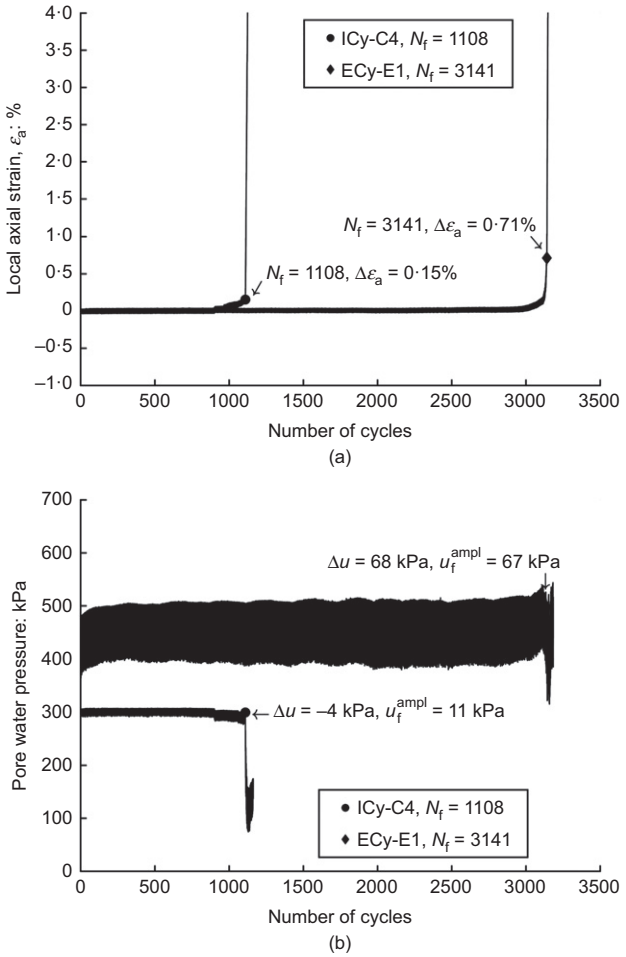

Fig. 11. (a) Cyclic axial strain and (b) pore water pressure trends for tests ICy-C4 and ECy-E1 performed at in situ and elevated stresses, denoting axial strains (ε_a) and pore water pressure (PWP) at the end of the N_f cycle, and the PWP amplitudes (u_f^{ampl}) for the N_f cycle

and then little further growth. No test exhibited an overall axial strain rate higher than the limit of 0·005% per day applying at the end of the creep stages imposed before cycling. The final ε_a/N ratios fell between 0·2 and $1{\cdot}6 \times 10^{-7}$%.

Data are presented in Fig. 12(b) from four intermediate experiments, ICy-C2 to ICy-C4 and ECy-E1, up to the cycle before they failed. ICy-C4 showed only minor permanent strains up to around 900 cycles, after which its rate of strain accumulation grew. The two other experiments showed less continuous trends, which are interpreted as reflecting discontinuities undergoing limited local pre-failure displacements. However, even in these cases the overall permanent strains and strain ratios remained relatively low before the onset of brittle failure. While these ultimately unstable tests' ε_a/N_f ratios were orders of magnitude higher (6·8 to 25×10^{-5}%) just before failure than those of the stable 'visco-elastic' group, they did not present any systematic relationship with N or the cyclic loading parameters.

The remaining five cases (ICy-D1 to ICy-D4 and ECy-F1) covered the highest cyclic loading levels. They failed after fewer cycles (see Fig. 12(c)) and gave the highest ε_a/N_f ratios. ECy-F1, which was cycled under the highest $q_{max}/(2S_u)$ of 0·94, failed after five cycles with $\varepsilon_a/N_f = 10^{-2}$%.

Higher cyclic loading levels generally led to lower cyclic stiffness, in keeping with the typically convex stress–strain behaviour shown by most geomaterials. The average cyclic E^u for the first cycles from the stable group (excluding ICy-C1) was 4·1 GPa, while the middle group's average was 3·4 GPa and the most highly loaded group (excluding ICy-D2-R) gave

3·3 GPa, all far exceeding the monotonic secant stiffness of 0·43 to 0·9 GPa indicated for shearing from in situ stresses in Fig. 5. The average damping ratios for the first cycles were 4·4 ± 1·5%, corresponding to cyclic strain range of 0·007–0·05%, showing no systematic variation between the test groups. The high damping ratios shown in Table 4 for ICy-B4 and ICy-D4, as well as for ECy-E1 and ECy-F1, reflect the response to the high q_{cyc}/q_{mean} ratios applied, which approach or equal unity. The stress–strain loops showed concave responses with significant curvature over the low q range, resembling those observed in Fig. 5 for monotonic loading stages. The ECy and ICy series' cyclic stiffnesses differed by far less than was seen during monotonic shearing from isotropic conditions. These and other aspects of the stiffness and damping behaviour may be associated with the micro-fissures identified in samples by Vinck *et al.* (2022) by Lawrence *et al.*'s (2018) technique. Advanced 'in situ' micro-CT techniques might identify micro-fissure patterns that correlate with mechanical behaviour. However, such scanning was not feasible within the programme.

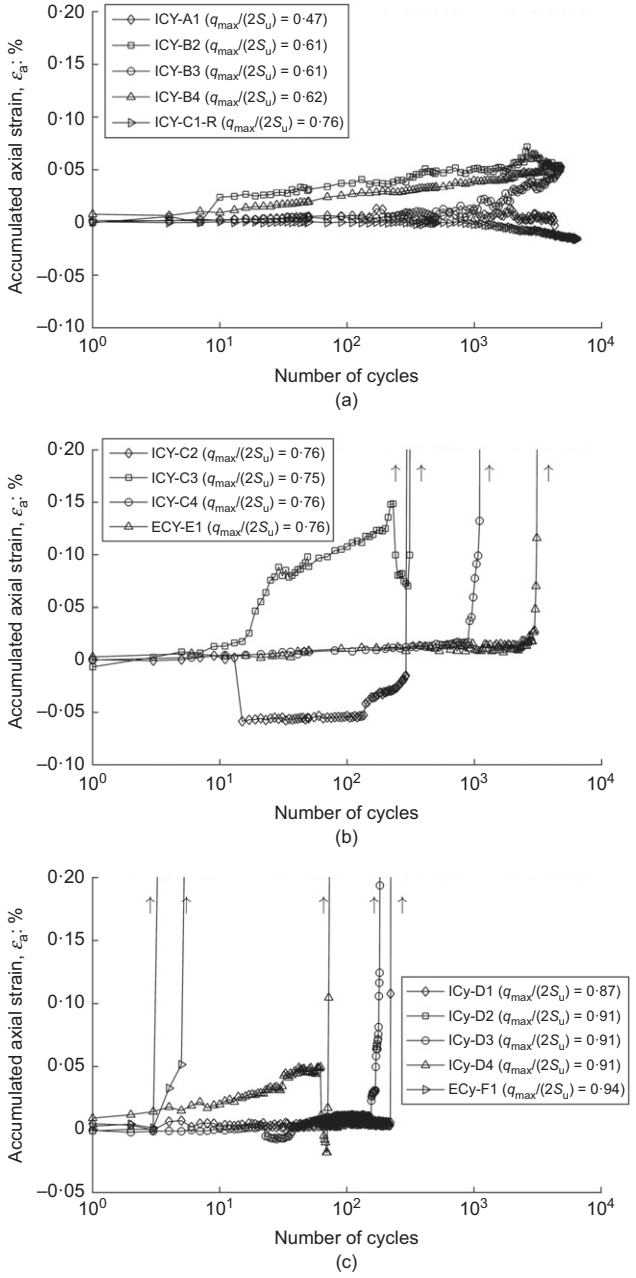

Fig. 12. Development of permanent strains during cycling: (a) stable 'group 1' tests ICy-A1 to ICy-C1-R, excluding ICy-C1; (b) unstable 'group 2' tests ICy-C2 to ICy-C4 and ECy-E1; and (c) unstable 'group 3' tests ICy-D1 to ICy-D4 and ECy-F1, excluding ICy-D2-R

Post-cyclic monotonic shear

The five specimens that met the local strain uniformity criterion and survived cyclic loading were subjected to post-cyclic monotonic tests. All reached peak strengths after small axial strain and minor pore pressure changes. Table 5 summarises the specimens' initial Young's moduli (E^u_{max}), as well as the secant stiffnesses, modest strains and small overall pore pressure changes applying at the points where samples failed with $q = q_f$. Their mean S_u (1211 kPa ± 10%) falls close to that given for monotonically tested (uncycled) specimens in Table 1, showing that long-term stable stress cycling has little impact on shear strength. However, the cycling boosted stiffness, possibly by further closing micro-discontinuities. The maximum monotonic E^u_{max} of specimens that had survived cycling exceeded the initial ($N = 1$) cyclic stiffnesses listed in Table 4. Two specimens, ICy-B4 and ICy-B3, which had been subjected to the highest $q_{cyc}/(2S_u)$ levels of 0·30 and 0·23 among this 'stable' group, showed remarkably stiffer responses on post-cyclic monotonic shearing, even though their initial cyclic stiffnesses had been unremarkable.

DISCUSSION

Figure 4 identified the cyclic loading conditions below which the intact chalk could sustain thousands of cycles without any deleterious effect, as well as those under which failures could be expected above the $N = 3000$ line. Fully stable behaviour has also been observed with sands and clays (Aghakouchak *et al.*, 2015; Ushev & Jardine, 2022), although over more restricted cyclic stress ranges. However, the abrupt undrained failures of the unstable chalk tests are unlike those observed with saturated soils, where cyclic failure develops once the effective stresses have reduced sufficiently to meet the (rate-adjusted) monotonic yielding criteria. With soils, cyclic collapse is usually preceded by pore pressure rises, permanent strain accumulation, loss of cyclic stiffness and growing damping ratios. In contrast, the intact chalk provided little indication of damage accumulating before cyclic failure. Collapse appears to reflect changes in the chalk's internal structure that only led to observable and progressive increases in strain rates as the tests approached failure. Similar features

Table 5. Summary of the key outcomes for the post-cyclic monotonic tests

Test	q_{mean}: kPa	E^u_{max}: GPa	E^u_{sec} at q_f: GPa	Mean ε_a: %	Δu: kPa	q_f: kPa	S_u: kPa
ICy-A1	760	4·4	3·8	0·05	2·6	2661	1211 (±120)
ICy-B2	1225	4·5	1·9	0·05	2·1	2250	
ICy-B3	910	7·9	3·8	0·04	0·7	2291	
ICy-B4	750	14·5	4·8	0·03	1·1	2457	
ICy-C1-R	1575	5·2	4·6	0·02	2·7	2453	

were noted in cyclic tests on artificially cemented calcarenites by Acharya (2004). However, the natural chalk tests showed a more marked tendency for local discontinuities to open or propagate as failure developed, leading to sharp pore pressure reductions and non-uniform displacements before the onset of overall failure.

Rather than resembling the cyclic response of saturated granular media, the intact chalk's behaviour appears closer to that of granites or marbles, and solids such as metals, glass or concrete – where load cycling above certain threshold levels initiates micro-shearing or cracking around inherent micro-features that generate stress concentrations. The latter initiators include micro-voids, discontinuities, sharp edges or imperfections in specimen geometry (Kranz, 1983; Suresh, 1991). In rocks, repeated loading prompts progressive wear and shearing between grains, forming microcracks that propagate within the matrix before coalescing into macro-cracks (Cerfontaine & Collin, 2018). Each load cycle within the unstable region leads to flaws growing at rates that depend on the cyclic amplitudes, mean loads and frequency, as well as confining pressures and any prior overloading in such media; raised temperature and humidity increase crack growth rates (Suresh, 1991). Acoustic emission signals and wave velocities provide indicators of fatigue damage in rock (Heap *et al.*, 2010; Xiao *et al.*, 2010), while metals can be scanned for micro-cracks and slips or monitored through electrical resistivity probing. However, the effects of cycling on rock specimens' response to uniaxial testing appeared hardly discernible in the triaxial tests until shortly before abrupt fatigue failure that broke cemented bonds and, when taken to the extreme, degraded specimens into unbonded material.

The triaxial test outcomes for chalk can be interpreted as '*S*–*N*' curves that plot the maximum cyclic load ($q_{max} = q_{mean} + q_{cyc}$) against log$N$ in a similar way to fatigue tests on hard rocks, metals or glass, with contours interpolated to show how the $q_{max}/(2S_u)$ curves fall as q_{cyc}/q_{mean} rises. Fig. 13 shows a family of contours of limiting $q_{max}/(2S_u)$ values applying at specified q_{cyc}/q_{mean} ratios. The relationships plotted are compatible with the fan of N_f contours proposed tentatively in Fig. 4, which follow equation (1), whose function relating to N_f is independent of q_{cyc}/q_{mean}

$$q_{cyc} = f(N)(2S_u - q_{mean}) \tag{1}$$

Although the linear N_f contours only apply to one-way conditions positioned to the right of the $q_{mean} = q_{cyc}$ boundary, as emphasised earlier, the $f(N)$ represents for each N_f line its projected intercept on the vertical axis of the interactive $q_{cyc}/(2S_u)$–$q_{mean}/(2S_u)$ diagram. The maximum cyclic stress can be expressed as equation (2).

$$\frac{q_{max}}{2S_u} = f(N)\frac{1 + q_{cyc}/q_{mean}}{f(N) + q_{cyc}/q_{mean}} \tag{2}$$

A tentative $f(N)$ function was found by considering the scatter of experimental outcomes for $f(N)$, as shown in Fig. 13, with the data points plotted in Fig. 4. Equation (3) is proposed as representing the trends in both figures and incorporates a lower limit of 0·35 for $f(N)$ under one-way loading. The lower limit corresponds to a fatigue limit (or fatigue strength) of $q_{max}/(2S_u) = 0{\cdot}52$ below which the specimens could sustain infinite cycles under the considered to be most critical $q_{cyc}/q_{mean} = 1$ one-way loading condition.

$$f(N) = 0{\cdot}35 + \frac{1}{1{\cdot}54 + 0{\cdot}37 \times [\log_{10}(N_f)]^{2{\cdot}75}} \tag{3}$$

Equation (3) is applicable to regular cycling with q_{cyc}/q_{mean} values no greater than unity. It offers a basis for empirical modelling of how the shear strength or yielding properties of chalk diminish under such conditions; Fig. 14 provides a three-dimensional representation of equation (2) combined with equation (3). Potential inhomogeneity and variation are recognised as major challenges in interpreting rock fatigue and constructing generalised *S*–*N* curves, adding to any

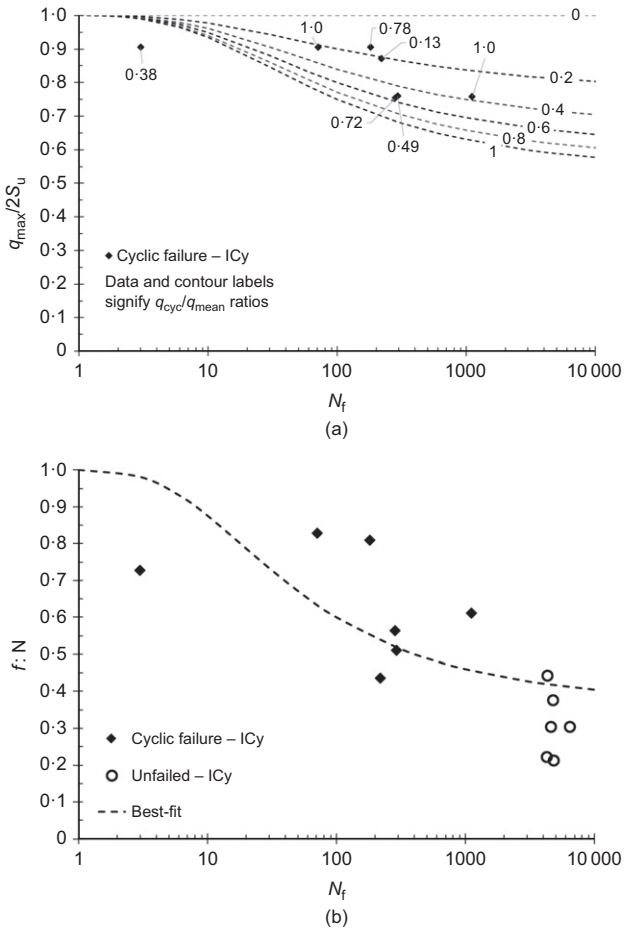

Fig. 13. Experimental data against interpretive trends: (a) *S*–*N* plot and q_{cyc}/q_{mean} contour lines; (b) $f(N)$–*N* data and the fitting trend

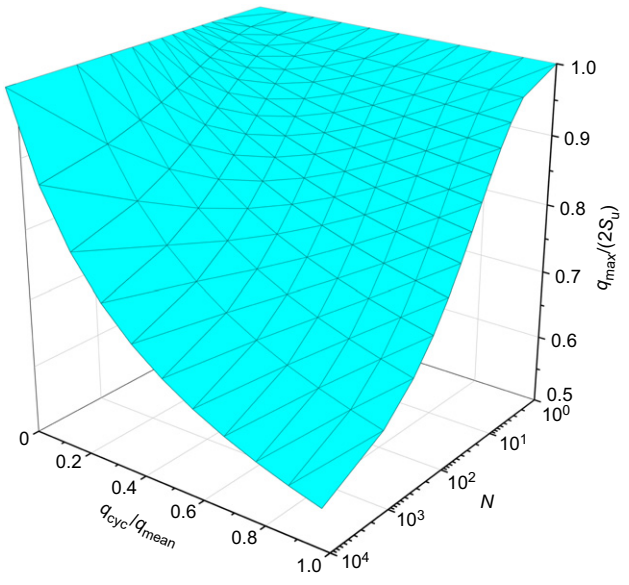

Fig. 14. Three-dimensional representation of the $q_{max}/(2S_u)$–q_{cyc}/q_{mean}–$\log_{10}(N)$ correlation

impact of experimental factors such as specimen size, saturation degree, anisotropy, cycling frequency and waveform (Acharya, 2004; Cerfontaine & Collin, 2018).

Alternative approaches exist for characterising the cyclic behaviour of cemented soils. These include Acharya's (2004) modification of the 'fatigue analysis ratio' S employed for metals to $S = q_{cyc}/(q_{peak} - q_{mean})$, which aims to cater for the influence of mean load. Vipulanandan & Ata (2000) have also applied probabilistic 'S–N–P' treatments developed to address concrete fatigue test specimen variability, although statistical treatments require relatively large datasets to be viable. Physically based frictional or other micro-macro-mechanical models have also been developed for describing fatigue in rocks by Scholz & Kranz (1974) and David *et al*. (2012). It is, at present, difficult to develop similarly fundamental models for low- to medium-density chalk. More information is needed to capture damage developing through micro-slips and/or crack propagation and cyclic failure characteristics under different q_{mean} and q_{cyc} combinations, as well as the more 'soil-like' features that become progressively more important under elevated stresses. Microscope examination of multiple specimens dismantled after different numbers of cycles (involving ranges of loading parameters) or micro-CT or other scanning (as employed by Yang *et al*. (2015)) during testing would help to elucidate these cyclic degradation processes.

Finally, it is important to recall that while the present tests imposed slow one-way stress-controlled cycles, large-displacement, two-way simple shear testing can degrade the chalk more dramatically to low-strength putty. Liu *et al*.'s (2022) parallel study considered how dynamically destructured chalk responds under cyclic loading after reconsolidation to stresses comparable to those applied in the thin annulus of putty that forms around the shafts of piles driven in chalk.

SUMMARY AND CONCLUSIONS

Only limited information exists on how cyclic loading affects the behaviour of natural chalk. This paper employs 20, long-term, high-resolution undrained monotonic and cyclic triaxial tests to investigate how nominally identical specimens of intact low- to medium-density structured chalk respond to stress-controlled, one-way, sinusoidal deviatoric loading. The tests identify the combinations of cyclic deviator and mean stress conditions below which the intact chalk can sustain thousands of cycles without any deleterious effect, as well as the conditions under which failures develop under specified numbers of cycles through tentative linear contours defined in an interactive cyclic failure scheme.

The chalk's cyclic response differs markedly from that of saturated unbonded soils, whose undrained cyclic collapses involve large pore pressure rises, permanent strain accumulation, cyclic stiffness losses, growing damping ratios and often progressive reductions in S_u. Instead, chalk's cyclic response appears to be closer to that of strongly cemented calcarenites, harder rocks and solids, such as metals or glass, where micro-shearing or cracking starts around inherent features that generate stress concentrations, and progressive wear and shearing between grains eventually leads to fatigue failure. The different main points that must be captured in any empirical or mechanics-based model of chalk's response to cyclic loading include the following.

(*a*) There are micro-fissures present in all samples. Their closure with increasing pressure appears to affect stiffness and damping behaviour, while their opening during unstable cycling contributes to brittle failure and the observed sharp pore pressure reductions.

(*b*) There is variability – the monotonic and cyclic outcomes are subject to scatter of around ± 12% in maximum stresses applied due to individual specimens' microstructure and geometrical imperfections.

(*c*) Nearly visco-elastic behaviour applies over the stable regions, which covers much of the interactive stress space considered. Stiffness improves in this region over thousands of cycles of long duration, without any loss of undrained shear strength.

(*d*) There is a sudden onset of cyclic failure. Intact chalk provides little indication of cyclic damage developing until shortly before failure, especially in tests conducted from in situ stresses. Collapse appears to involve changes in the chalk's internal structure that only become apparent as failure approaches.

(*e*) There is an impact from elevating pressures. Specimens consolidated 300 kPa above in situ mean stresses manifest higher pre-cycling monotonic stiffness values, more positive cyclic pore pressure changes and significantly less dilative trends as cyclic failure develops. However, their abrupt failure patterns are compatible with the 'in situ' pressure level tests and do not show greater sensitivity to cycling at given levels of loading.

ACKNOWLEDGEMENTS

The study was undertaken under the ALPACA project funded by the Engineering and Physical Science Research Council (EPSRC) grant EP/P033091/1, Royal Society Newton Advanced Fellowship NA160438 and Supergen ORE Hub 2018 (EPSRC EP/S000747/1). Byrne is supported by the Royal Academy of Engineering under the Research Chairs and Senior Research Fellowships scheme. The authors acknowledge additional financial and technical support by Atkins, Cathie Associates, Equinor, Fugro, Geotechnical Consulting Group (GCG), Iberdrola, Innogy, LEMS, Ørsted, Parkwind, Siemens, TATA Steel and Vattenfall. Imperial College's EPSRC Centre for Doctoral Training (CDT) in Sustainable Civil Engineering and the DEME Group (Belgium) supported Ken Vinck. Socotec UK Ltd and Fugro carried out the block sampling and rotary core sampling campaigns. Invaluable technical support by Steve Ackerley, Graham Keefe, Prash Hirani, Stef Karapanagiotidis, Graham Nash and Gary Jones at Imperial College is acknowledged gratefully.

NOTATION

$A_{elastic}$	unloading half-cycle elastic triangle area with height as q_{cyc} ($= (q_{peak} - q_{trough})/2$) and width as cyclic strain ($= (\varepsilon_{peak} - \varepsilon_{trough})/2$)
A_{loop}	area enclosed by a stress–strain (q–ε_a) loop for a complete sinusoidal stress cycle
c'	soil cohesion
D	damping ratio ($= A_{loop}/(4\pi A_{elastic})$)
D_{50}	mean particle diameter
E^u_{max}	maximum undrained Young's moduli
E^u_{sec}	undrained secant vertical Young's modulus
$E^{u,cyc}_{sec}$	cyclic undrained secant vertical Young's modulus
e_0	specimen initial void ratio
G_s	specific gravity
K_0	earth pressure coefficient at rest
M	critical state q/p' stress ratio
N	number of cycles
N_f	number of cycles to failure
p'	mean effective stress
p'_0	initial mean effective stress
Q	deviatoric stress

q_{cyc} cyclic deviatoric stress amplitude ($= (q_{peak} - q_{trough})/2$)
q_f deviatoric stress at failure
q_{max} maximum q applied in stress cycle ($= q_{mean} + q_{cyc}$)
q_{mean} mean q applied in stress cycle
q_{peak} peak q applied in stress cycle ($= q_{max}$)
q_{trough} minimum q applied in stress cycle ($= q_{mean} - q_{cyc}$)
S_r saturation degree
S_u undrained shear strength
u_f^{ampl} pore water pressure amplitude at the failure cycle
Δu excess pore water pressure
ε_a axial (vertical) strain
ε_{peak} axial strain at q_{peak}
ε_r radial (horizontal) strain
ε_s shear strain ($= \varepsilon_a$ for undrained triaxial condition)
ε_{trough} axial strain at q_{trough}
ϕ'_{cs} critical state shear resistance angle
ϕ'_{peak} shear resistance angle at peak

REFERENCES

Acharya, S. S. (2004). *Characterisation of cyclic behaviour of calcite cemented soils.* PhD thesis, University of Western Australia, Perth, Australia.

Aghakouchak, A., Sim, W. W. & Jardine, R. J. (2015). Stress-path laboratory tests to characterise the cyclic behaviour of piles driven in sands. *Soils Found.* **55**, No. 5, 917–928.

Andersen, K. (2009). The 21st Bjerrum lecture: bearing capacity under cyclic loading – offshore, along the coast, and on land. *Can. Geotech. J.* **46**, No. 5, 513–535.

Andersen, K. (2015). Cyclic soil parameters for offshore foundation design. In *Frontiers in offshore geotechnics III: proceedings of the 3rd international symposium on frontiers in offshore geotechnics (ISFOG 2015)* (ed. V. Meyer), vol. 1, pp. 5–82. London, UK: CRC Press/Balkema (Taylor & Francis Books Ltd).

ASTM (2019). D4543-19: Standard practices for preparing rock core as cylindrical test specimens and verifying conformance to dimensional and shape tolerances. West Conshohocken, PA, USA: ASTM International.

Carrington, T. M., Li, G. & Rattley, M. J. (2011). A new assessment of ultimate unit friction for driven piles in low to medium density chalk. In *Proceedings of the 15th European conference on soil mechanics and geotechnical engineering: geotechnics of hard soils – weak rocks* (eds A. Anagnostopoulos, M. Pachakis and C. Tsatsanifos), Part 4, pp. 825–830. Amsterdam, the Netherlands: IOS Press.

Cerfontaine, B. & Collin, F. (2018). Cyclic and fatigue behaviour of rock materials: review, interpretation and research perspectives. *Rock Mech. Rock Engng* **51**, No. 2, 391–414.

Coyne, D. L., Rattley, M., Houlston, P., Alobaidi, I., Benson, A. & Russell, C. (2015). Cyclic laboratory testing of chalk to improve the reliability of piled foundation design. In *Frontiers in offshore geotechnics III: proceedings of the 3rd international symposium on frontiers in offshore geotechnics (ISFOG 2015)* (ed. V. Meyer), vol. 1, pp. 1185–1190. London, UK: CRC Press/Balkema (Taylor & Francis Books Ltd).

David, E. C., Brantut, N., Schubnel, A. & Zimmerman, R. W. (2012). Sliding crack model for non-linearity and hysteresis in the uniaxial stress–strain curve of rock. *Int. J. Rock Mech. Min. Sci.* **52**, 9–17.

Heap, M. J., Faulkner, D. R., Meredith, P. G. & Vinciguerra, S. (2010). Elastic moduli evolution and accompanying stress changes with increasing crack damage: implications for stress changes around fault zones and volcanoes during deformation. *Geophys. J. Int.* **183**, No. 1, 225–236.

Ishihara, K. (1996). *Soil behaviour in earthquake geotechnics.* Oxford, UK: Oxford University Press.

Jardine, R. J., Brooks, N. J. & Smith, P. R. (1985). The use of electrolevel transducers for strain measurements in triaxial tests on weak rock. *Int. J. Rock Mech. Min. Sci. & Geomech. Abs.* **22**, No. 5, 331–337.

Jardine, R. J., Puech, A. & Andersen, K. H. (2012). Cyclic loading of offshore piles: potential effects and practical design. In *Offshore site investigation and geotechnics: integrated technologies – present and future*, pp. 59–97. London, UK: Society of Underwater Technology.

Jardine, R. J., Kontoe, S., Liu, T., Vinck, K., Byrne, B. W., McAdam, R. A., Schranz, F., Andolfsson, T. & Buckley, R. M. (2019). The ALPACA research project to improve design of piles driven in chalk. In *Proceedings of the 17th European conference on soil mechanics and geotechnical engineering – geotechnical engineering, foundation of the future* (eds H. Sigursteinsson, S. Erlingsson and B. Bessason), paper 71. Reykjavik, Iceland: The Icelandic Geotechnical Society.

Kohata, Y., Tatsuoka, F., Wang, L., Jiang, G. J., Hoque, E. & Kodaka, T. (1997). Modelling the non-linear deformation properties of stiff geomaterials. *Géotechnique* **47**, No. 3, 563–580, https://doi.org/10.1680/geot.1997.47.3.563.

Kranz, R. L. (1983). Microcracks in rocks: a review. *Tectonophysics* **100**, No. 1, 449–480.

Lagioia, R. & Nova, R. (1995). An experimental and theoretical study of the behaviour of a calcarenite in triaxial compression. *Géotechnique* **45**, No. 4, 633–648, https://doi.org/10.1680/geot.1995.45.4.633.

Larsen, S. P., Katić, N. & Trads, N. (2017). Cyclic testing on low-density chalk. In *Advances in laboratory testing and modelling of soils and shales* (eds A. Ferrari and L. Laloui), pp. 359–366. Cham, Switzerland: Springer.

Lawrence, J. A., Mortimore, R. N. & Thrower, A. (2018). Macro and micro fabrics in chalk identified using the Bushinsky Oil Technique: an updated method and new applications for an old experimental technique. In *Engineering in chalk: proceedings of the chalk 2018 conference* (eds J. A. Lawrence, M. Preene, U. L. Lawrence and R. M. Buckley), pp. 549–555. London, UK: ICE Publishing.

Le, T. M. H., Eiksun, G. R., Strøm, P. J. & Saue, M. (2014). Geological and geotechnical characterisation for offshore wind turbine foundations: a case study of the Sheringham Shoal wind farm. *Engng Geol.* **177**, 40–53.

Leroueil, S. & Vaughan, P. R. (1990). The general and congruent effects of structure in natural soils and weak rocks. *Géotechnique* **40**, No. 3, 467–488, https://doi.org/10.1680/geot.1990.40.3.467.

Liu, T., Ahmadi-Naghadeh, R., Vinck, K., Jardine, R. J., Kontoe, S., Buckley, R. M. & Byrne, B. W. (2022). An experimental investigation into the behaviour of de-structured chalk under cyclic loading. *Géotechnique*, https://doi.org/10.1680/jgeot.21.00199.

Maqsood, Z., Koseki, J. & Kyokawa, H. (2019). Effects of loading rate on strength and deformation characteristics of gypsum mixed sand. In *Proceedings of 7th international symposium on deformation characteristics of geomaterials (IS-Glasgow 2019)* (eds A. Tarantino and E. Ibraim), E3S Web of Conferences vol. 92, paper 05008 (2019). Les Ulis, France: EDP Sciences.

Scholz, C. H. & Kranz, R. (1974). Notes on dilatancy recovery. *J. Geophys. Res.* **79**, No. 14, 2132–2135.

Suresh, S. (1991). *Fatigue of materials.* Cambridge, UK: Cambridge University Press.

Tatsuoka, F., Jardine, R. J., Lo Presti, D., Di Benedetto, H. & Kodaka, T. (1999). Theme lecture: characterising the pre-failure deformation properties of geomaterials. In *Proceedings of the 14th international conference on soil mechanics and foundation engineering*, pp. 2129–2164. Rotterdam, the Netherlands: Balkema.

Ushev, E. R. & Jardine, R. J. (2022). The behaviour of Bolders bank glacial till under undrained cyclic loading. *Géotechnique* **72**, No. 1, 1–19, https://doi.org/10.1680/jgeot.18.P.236.

Vinck, K. (2021). *Advanced geotechnical characterisation to support driven pile design at chalk sites.* PhD thesis, Imperial College, London, UK.

Vinck, K., Liu, T., Ushev, E. & Jardine, R. J. (2019). An appraisal of end conditions in advanced monotonic and cyclic triaxial testing on a range of geomaterials. In *Proceedings of 7th international symposium on deformation characteristics of geomaterials (IS-Glasgow 2019)* (eds A. Tarantino and E. Ibraim), E3S Web of Conferences vol. 92, paper 02007 (2019). Les Ulis, France: EDP Sciences.

Vinck, K., Liu, T., Jardine, R. J., Kontoe, S., Ahmadi-Naghadeh, R., Buckley, R. M., Byrne, B. W., Lawrence, J., Mcadam, R. A. & Schranz, F. (2022). Advanced in situ and

laboratory characterisation of the ALPACA chalk research site. *Géotechnique* in press, https://doi.org/10.1680/jgeot.21.00197.

Vipulanandan, C. & Ata, A. (2000). Cyclic and damping properties of silica grouted sand. *J. Geotech. Geoenviron. Engng* **126**, No. 7, 650–656.

Wichtmann, T., Niemunis, A. & Triantafyllidis, T. (2005). Strain accumulation in sand due to cyclic loading: drained triaxial tests. *Soil Dyn. Earthq. Engng* **25**, No. 11, 967–979.

Xiao, J. Q., Ding, D. X., Jiang, F. L. & Xu, G. (2010). Fatigue damage variable and evolution of rock subjected to cyclic loading. *Int. J. Rock Mech. Min. Sci.* **47**, No. 3, 461–468.

Yang, S. Q., Ranjith, P. G., Huang, Y. H., Yin, P. F., Jing, H. W., Gui, Y. L. & Yu, Q. L. (2015). Experimental investigation on mechanical damage characteristics of sandstone under triaxial cyclic loading. *Geophys. J. Int.* **201**, No. 2, 662–682.